International Journal of Refrigeration 131 (2021) 381–393

Contents lists available at ScienceDirect

International Journal of Refrigeration

journal homepage: www.elsevier.com/locate/ijrefrig

An analytical design tool for pin fin sorber bed heat/mass exchanger

Outil de conception analytique pour un échangeur de chaleur/masse à lit absorbant à ailettes à picots

MJ. Darvish, H. Bahrehmand, M. Bahrami *

Laboratory for Alternative Energy Conversion (LAEC), School of Mechatronic Systems Engineering, SFU, BC, CA V3T OA3

ARTICLE INFO

Keywords:
Sorption system
analytical modeling
heat and mass transfer
coefficient of performance
specific cooling power

Mots clés:
Système à sorption
Modélisation analytique
Transfert de chaleur et de masse
Coefficient de performance
Puissance de refroidissement spécifique

ABSTRACT

This paper proposes a novel closed-form analytical model to predict the sorption performance of a pin fin heat/mass exchanger (PF-HMX) prototype, using the Eigenfunction expansion method to solve the governing energy equation. The proposed transient 2-D solution includes all salient thermophysical and sorption properties, sorbent geometry, operating conditions, and the thermal contact resistance at the interface between the sorber bed heat exchanger and sorption composite. An analysis of variance (ANOVA) method is utilized to understand the percentage contribution of each parameter on specific cooling power (SCP) and coefficient of performance (COP). It is shown that the amount of graphite flake, sorbent thickness, and fin radius on one hand and cycle time and graphite flake content on the other have the highest level of contribution to the COP and SCP, respectively. Moreover, a parametric study found that HMX geometry, sorbent properties, and cycle time counteract effects on COP and SCP, which should be optimized simultaneously to build an optimal design. The analytical model was validated successfully using the sorption data from a custom-built gravimetric large temperature jump (G-LTJ) testbed. The experimental results show that the present PF-HMX design with a relatively low mass ratio (MR) can achieve an SCP of 1160 W kg^{-1} and a COP of 0.68 which are higher than the previously published results in the literature.

1. Introduction

The heating and cooling systems consume over 60% of the residential and almost 50% of the commercial building energy (Ürge-Vorsatz et al., 2015). Powered by electricity, vapor-compression systems (VCR) are the most common cooling technologies in the market. And since more than 80% of the global energy– including electrical power generation (Askalany et al., 2013, Pridasawas, 2006)– is generated from fossil fuels, building heating and cooling systems are major greenhouse gas emitters (Cullen and A, 2010), which leads to catastrophic environmental impact including the climate change.

Furthermore, fluorocarbon-type refrigerants used in VCR systems are not only potent greenhouse gases but also implicated in ozone depletion (Pinheiro et al., 2016, Demir et al., 2008).

52% of the global primary energy is lost as waste heat (Forman et al., 2016), with low-grade energies (temperature sources below 100°C) constituting 63% of this untapped energy (Forman et al., 2016). Sorption Waste-heat-driven cooling/heating systems have the potential to offer a solution to world energy needs and reducing environmental pollutants. Sorption cooling and heating systems (SCHS) have recently drawn immense attention as an alternative technology that enhances the efficiency of energy systems to reduce reliance on fossil fuels for heating and cooling. However, they have not been widely adopted due to the following: i) low thermal conductivity and diffusivity of the sorbent composites; ii) low heat and mass transfer due to the inefficiency of existing sorber bed heat exchanger designs; and iii) low operating pressure (near vacuum), all of which lead to large, inefficient, and costly SCHS (Zhao et al., 2012, Wu et al., 2009, Sharafian et al., 2016, Hu et al., 1997, Saha et al., 2006).

To address some of these challenges, this study evaluates a new PF-HMX sorber bed design proposed as an alternative to off-the-shelf sorbers. The proposed PF-HMX can provide both high COP and enhanced heat and mass transfer inside the sorber bed. To assess the

* Corresponding author. Prof. Majid Bahrami, School of Mechatronic Systems Engineering, Simon Fraser University, 250-13450 102 Avenue, Surrey, BC, V3T 0A3, Canada. Tel: +1 (778) 782-8538; Fax: +1 (778) 782-7514.
E-mail addresses: mrajabta@sfu.ca (MJ. Darvish), sbahrehm@sfu.ca (H. Bahrehmand), mbahrami@sfu.ca (M. Bahrami).

https://doi.org/10.1016/j.ijrefrig.2021.07.027
Received 6 May 2021; Received in revised form 20 July 2021; Accepted 21 July 2021
Available online 20 August 2021
0140-7007/

Nomenclature

A	heat transfer area, m^2
Bi	heat transfer Biot number
c	specific heat capacity, J kg^{-1} K^{-1}
Fo	Fourier number
H	height, m
h	convective heat transfer coefficient, W m^{-2} K^{-1}
H_{ads}	enthalpy of adsorption, J kg^{-1}
h_{fg}	enthalpy of evaporation, J kg^{-1}
k	thermal conductivity, W m^{-1} K^{-1}
L	height of adsorbent, m
p	pressure, Pa
p_o	saturation pressure, Pa
R	radius, m
Δ	thickness, m
t	time, s
r	radial coordinate
T	temperature, K
z	coordinate
R	thermal resistance, K m^2 W^{-1}

Greek

λ	eigenvalue in η direction for mass diffusion problem
β	eigenvalue in η direction for heat transfer problem
γ	eigenvalue in ξ direction for heat transfer problem
η	dimensionless coordinate of r
ξ	dimensionless coordinate of z
τ	cycle time, s
Θ	dimensionless temperature
κ	dimensionless thermal conductivity ratio
α	thermal diffusivity, m^2 s^{-1}
μ	dimensionless thermal diffusivity
Λ	dimensionless thermal contact conductance
ω	adsorbate uptake, (g $_{sorbate}$ $g^{-1}{}_{dry\ sorbent}$)

Subscripts

0	initial condition
ads	adsorption
c	channel
cond	condenser
des	desorption
evap	evaporator
eq	equilibrium
f	fin
fs	fin spacing
HTF	heat transfer fluid
s	sorbent

Subscripts

ANOVA	analysis of variance
COP	coefficient of performance
G-LTJ	gravimetric large temperature jump
MR	mass ratio
PF-HMX	pin fin heat and mass exchanger
PVA	polyvinyl alcohol
SCHS	sorption cooling and heating system
SCP	specific cooling power
TCR	thermal contact resistance
TGA	thermogravimetric sorption analyzer
TPS	transient plane source

performance of the proposed PF-HMX, we developed a predictive analytical closed-form model to provide an accurate and fast evaluation of SCHS performance as a function of the design, sorption material properties, and operating conditions.

A number of approaches have been proposed for the modeling of sorption systems in the literature. They can be categorized into three main modeling groups: (i) thermodynamic, (ii) lumped parameter, and (iii) conjugate heat and mass transfer analysis. Thermodynamic analysis (Henninger et al., 2012, Tamainot-Telto et al., 2009) is the simplest steady-state simulation in which details of heat and mass transfer are not considered; however, it can reveal the upper-limit performance of sorption systems. Lumped models (Saha et al., 2007, Pan et al., 2016, Ahmed and Al-Dadah, 2012, Rogala, 2017, Mitra et al., 2018) consists of three governing equations: sorption equilibrium, energy balance, and mass balance. The focus of this modeling approach is on the sorber bed as the geometrical details of the HMX cannot be included in the analysis. Other simplifying assumptions are: (i) a uniform temperature and pressure in the sorber bed, (ii) a uniform uptake in the bed, and (iii) a thermodynamic equilibrium for both gas and solid phases. The conjugate heat and mass transfer model considers the variation of temperature and mass content of the HMX in both time and space domains. The governing equations are expressed as the following partial differential

Table 1
A summary of the specification and performance of available studies with a reasonable compromise between SCP, COP, and MR. * HTF data was not available in the publication.

Ref	Sorption pair	S-HMX	t_{cycle} (min)	SCP (W kg^{-1})	COP	MR
(Freni, 2007)	Coating silica gel + $CaCl_2$(SWS-1l)/ water	Aluminum finned tube	10	137	0.15	4.47 *
(Dawoud et al., 2010)	Coating AQSOA-FAMZ02/ water	Extruded Aluminum finned-tube heat exchanger		295	0.21	5.37 *
(Sharafian, 2016)	Loose grain AQSOA-FAM Z02/water	Round tube-fin packed	20	120	0.3	7.86
(Sharafian, 2016)	Loose grain AQSOA-FAM Z02/water	Round tube-fin packed	20	70	0.45	3.29
(Aristov et al., 2010)	Loose grain LiNO3–Silica KSK/water (SWS-9l)	Aluminum finned flat tube	6.4	318	0.176	2.82 *
(Sapienza et al., 2011)	Loose grain AQSOA-FAM Z02/water	Aluminum finned flat tube	7	394	0.6	3.61
(Freni et al., 2015)	Coating zeolite, SAPO-34/water	Aluminum finned flat tube	5	675	0.24	10
(Freni et al., 2015)	Loose grain zeolite, SAPO-34/water	Aluminum finned flat tube	5	498	0.4	4.11
(Wittstadt et al., 2017)	Coating SAPO- 34/water	Aluminum sintered metal fiber structures soldered on flat fluid channels	10	852	0.4	4.15
(Bahrehmand and Bahrami, 2019)	Coating silica gel + $CaCl_2$/water	Aluminum plate-finned HMX	10	1005	0.6	4.7
(Bahrehmand and Bahrami, 2020)	Coating silica gel + $CaCl_2$/water	Aluminum finned-tube HMX	10	766	0.55	4

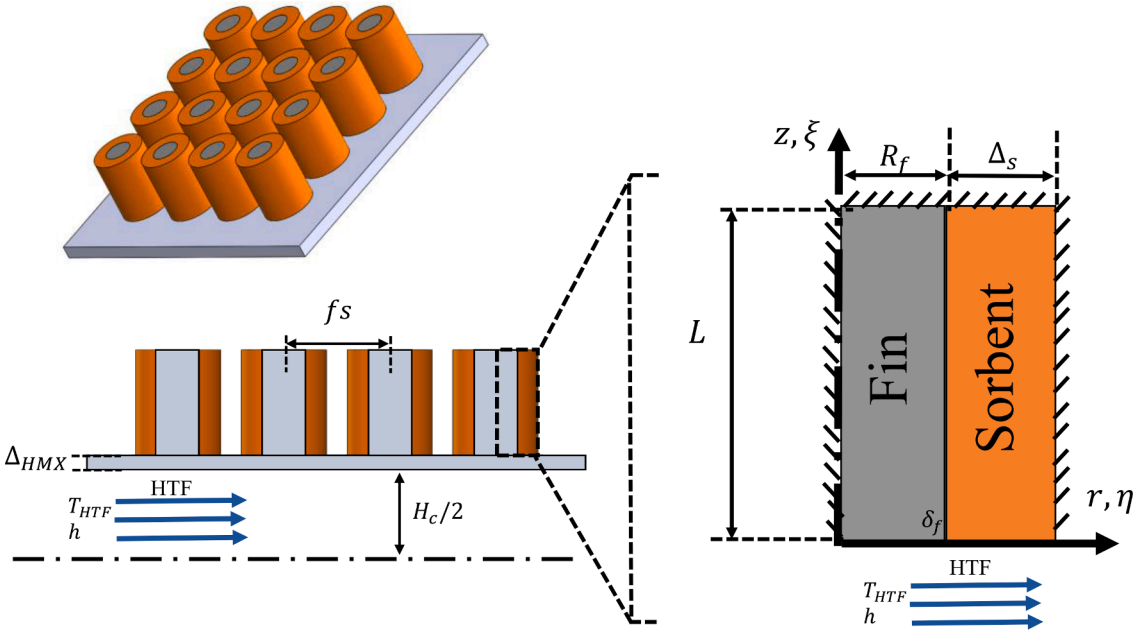

Fig. 1. Schematic of the solution domain consisting of sorbent coating and pin fin heat and mass exchanger, the in-line arrangement is shown. For dimensions of the PF-HMX see table 2.

equations with initial values and boundary conditions: (i) conservation of energy, (ii) conservation of mass, and (iii) state equation for the sorbent material. Due to the sorption kinetics and thermophysical properties, the aforementioned equations are transient, complex, and nonlinear. As such, finding a closed-form analytical solution for such conjugate heat and mass transfer is extremely challenging. Therefore, numerical methods are commonly used; examples include: i) finite difference method (Mitra et al., 2018, Guilleminot et al., 1987, Jribi et al., 2017, Alam et al., 2000, Amini and Steen, 2012, Amar et al., 1996, Zhang and Wang, 1999, El Fadar, 2015, Ndiaye et al., 2017, Duquesne et al., 2014, Solmus et al., 2012, Li et al., 2004), ii) finite volume method (Mhimid, 1998, Niazmand and Dabzadeh, 2012, Mohammed et al., 2017, Tatsidjodoung et al., 2016, Golparvar et al., 2018), and iii) finite element method (Passos et al., 1989, Mette et al., 2014, Aydin et al., 2018, Lele et al., 2014, Bhouri and Bürger, 2017, Fopah Lele et al., 2015, Hong et al., 2015, Çağlar, 2016); the key issue with numerical modeling is high computation time that makes optimization and control of the operational parameters in real-time application. There are a few analytical closed-form models in the literature that provide low computation time and high accuracy (Bahrehmand et al., 2018, Bahrehmand and Bahrami, 2019, Jeric and Nottage, 2012, Bahrehmand and Bahrami, 2020).

There are several studies in the literature with a focus on developing sorber beds. The specification and performance of these SCHS systems are summarized in table 1, which includes working pairs, sorber bed HMX design, reported SCP, COP, and MR. However, one can conclude that the literature lacks a closed-form solution that includes the geometry of HMX, salient thermophysical and sorption properties as well as operational input parameters and: (i) considers the transient behavior of sorber bed; and (ii) thermal contact resistance at the interface between the sorption material and the HMX.

A number of studies have been conducted to improve the heat transfer of the sorbent by adding thermally conductive additives [Demir et al., 2010; Rezk et al., 2013; Gediz Ilis et al., 2019; Khatibi et al., 2021]. To enhance the thermal diffusivity of the sorbent material, a consolidated composite, consisting of $CaCl_2$, silica gel B150, with added natural graphite flakes is prepared. The thermally conductive additive, natural graphite flakes, reduces the active sorbent fraction in the composite, creating a need for establishing an optimum composition for a specific application; more details can be found in our previous study (Bahrehmand et al., 2018).

The objective of this study is to propose and develop a novel sorber bed HMX design to provide a high SCP and COP with relatively low MR. To this end, a 2-D analytical solution is developed for a PF-HMX. In

To achieve this objective, first, a parametric study is carried out to examine the effect of key design and operating variables on the COP and SCP. Subsequently, an analysis of variance (ANOVA) is conducted to find the level of contribution of each parameter to the performance of the SCHS. Our proposed PF-HMX beds achieved a SCP of 1160 W kg^{-1}, a COP of 0.68, with a MR of 3.3, under the operating condition of a sorption chiller: T_{des}=90°C, T_{ads}=T_{cond}=30°C, and T_{evap}=15°C.

2. Performance parameters

SCP is defined as the evaporative cooling rate generated per mass of dry sorbent material and represents how fast the heat and mass transfer processes take place in the sorber bed, Eq. (1).

$$SCP = \frac{Q_{evap}}{m_s\ \tau} = \frac{m_s \int_{ads} \frac{d\omega}{dt} h_{fg} dt}{m_s\ \tau} = \frac{\Delta\omega\ h_{fg@T_{evap}}}{\tau} \tag{1}$$

where, Q_{evap} is the evaporative cooling energy (J), m_s is the sorbent mass (kg), ω is the sorbate uptake (g $_{sorbate}$ $g^{-1}_{sorbent}$), h_{fg} is the sorbate enthalpy of evaporation (J kg^{-1}), and τ is the cycle time (s).

COP, defined as the ratio of the evaporative cooling energy to the input energy, which is the summation of desorption heat and sensible heat, Eq. (2). COP can be increased by: (i) enhancing the heat and mass transfer rate in the sorber bed to increase both the evaporative cooling energy and the desorption heat, which overall increases COP, and (ii) decreasing the thermal inertia of the HMX, which reduces the (sensible) heat input needed to perform the temperature swing during the adsorption and desorption cycle.

$$COP = \frac{Q_{evap}}{Q_{input}} = \frac{Q_{evap}}{Q_{sens} + Q_{des}} = \frac{m_s \int_{ads} \frac{d\omega}{dt} h_{fg} dt}{\int_{ads} \left(\left(m_s \left(c_{p,s} + \omega\ c_{p,w} \right) + m_{HMX} c_{p,HMX} \right) \frac{dT}{dt} - m_s \frac{d\omega}{dt} H_{ads} \right) dt} \tag{2}$$

where, Q_{evap} is the evaporative cooling energy (J), Q_{input} is the input thermal energy (J), Q_{sens} is the thermal energy required to overcome thermal inertia of the sorber bed HMX (J), Q_{des} is the thermal energy consumed for desorption (J), m_s is the sorbent mass (kg), m_{HMX} is the mass of HMX (kg), ω is the sorbate uptake (g sorbate g^{-1} sorbent), h_{fg} is the sorbate enthalpy of evaporation (J kg^{-1}), H_{ads} is the enthalpy of adsorption (J kg^{-1}), c_p is the specific heat (J kg^{-1} K^{-1}), and T is the sorbent temperature (K).

In order to properly evaluate the performance of the sorption cooling system, the MR of sorber bed masses to sorbent material is also considered as follows:

$$MR = \frac{m_{HMX} + m_s + m_{HTF}}{m_s} \tag{3}$$

where m_{HMX} is the mass of HMX (kg), m_s is the sorbent mass (kg), and m_{HTF} is the heat transfer fluid (HTF) mass.

3. Model development

Based on the general approach reported in our lab's previous publications (Bahrehmand et al., 2018, Bahrehmand and Bahrami, 2019, Bahrehmand and Bahrami, 2020), a new 2-D analytical solution is proposed to determine the parameters inside the in-line arrangement of pin fin heat/mass exchanger; these include transient temperature distribution, heat transfer rate, uptake, and the sorption performance. Figure 1 shows the solution domain schematically which includes PF-HMX, HTF, and the sorbent material. The assumptions used to develop the model include:

- Two-dimensional, transient heat and mass transfer with constant thermo-physical properties,
- Constant temperature for the HTF, due to the relatively higher heat capacity of the heat transfer fluid (Wu et al., 2009),
- The boundaries of the sorbent and the fin that are in contact with low pressure refrigerant vapor are assumed to be adiabatic, i.e., due to the low Biot number (Wakao and Kagei, 1982)[8], and
- The radiative heat transfer is neglected because of the low temperature difference between the sorbent and surrounding (10-20 K).

From these assumptions, the energy equation can be written as follows for both sorbent and HMX fin.

$$\frac{\partial T_i}{\partial t} = \alpha_{i,r}\left(\frac{\partial^2 T_i}{\partial r^2} + \frac{1}{r}\frac{\partial T_i}{\partial r}\right) + \alpha_{i,z}\left(\frac{\partial^2 T_i}{\partial z^2}\right) + \frac{1}{(\rho c_p)_i}G_i(t),\ T_i(r,z,t),\ i = s,f \tag{4}$$

$$G_i(t) = \begin{cases} \rho_s H_{ads}\dfrac{d\omega}{dt}, & i = s \\ 0, & i = f \end{cases} \tag{5}$$

where, T_i is the temperature of the i^{th} layer (K), α is the thermal diffusivity for the i^{th} layer (m^2 s^{-1}), ρ is the density for the i^{th} layer (kg m^{-3}), c_p is the specific heat (J kg^{-1} K^{-1}), r and z are the coordinates, t is time (s), H_{ads} is the enthalpy of adsorption (J kg^{-1}), and G_i is the heat generation inside the i^{th} layer and i=s, and i=f represent the sorbent and HMX domains, respectively. The boundary conditions are:

$$\frac{\partial T_i(0,z,t)}{\partial r} = 0 \tag{6}$$

$$\frac{\partial T_s(\Delta_s + R_f, z, t)}{\partial r} = 0 \tag{7}$$

$$\frac{\partial T_i(r,L,t)}{\partial z} = 0 \tag{8}$$

$$\begin{aligned} R &= \frac{\Delta_{HMX}}{k_{f,z}} + \frac{1}{h} + TCR.A \\ \frac{1}{R}(T_s(r,0,t) - T_{HTF}) &= k_s\frac{\partial T_s(r,0,t)}{\partial z} \\ \frac{1}{R}(T_f(r,0,t) - T_{HTF}) &= k_{f,z}\frac{\partial T_f(r,0,t)}{\partial z} \end{aligned} \tag{9}$$

$$\begin{aligned} k_{f,r}\left(\frac{\partial T_f(R_f,z,t)}{\partial r}\right) &= k_s\frac{\partial T_s(R_f,z,t)}{\partial r} - k_{f,r}\left(\frac{\partial T_f(R_f,z,t)}{\partial r}\right) \\ &= \frac{1}{TCR.A}(T_f(R_f,z,t) - T_s(R_f,z,t)) \end{aligned} \tag{10}$$

where, T_i is the temperature of the i^{th} layer (K), Δ_s is the sorbent thickness (m), Δ_{HMX} is the HMX thickness (m), R_f is the fin radius (m), L is the fin height (m), A is the heat transfer area (m^2), k is the thermal conductivity for the i^{th} layer (W m^{-1} K^{-1}), h is the convective heat transfer coefficient (W m^{-2} K^{-1}), r and z are the coordinates, t is time (s), and TCR is the thermal contact resistance between fin and sorbet.

The initial condition for temperature is

$$T_i(r,z,0) = T_0 \tag{11}$$

Non-dimensional variables were defined:

$$\eta = \frac{r}{R_f + \Delta_s} \qquad \xi = \frac{z}{L} \qquad Fo = \frac{t\alpha_z}{L^2} \qquad \theta_i = \frac{T_i - T_{HTF}}{T_0 - T_{HTF}}$$

$$\delta = \frac{L}{R_f + \Delta_s} \qquad \delta_f = \frac{R_f}{R_f + \Delta_s} \qquad \mu_r^2 = \frac{\alpha_r}{\alpha_z} \qquad \mu_s^2 = \frac{\alpha_s}{\alpha_z}$$

$$\kappa = \frac{k_s}{k_{f,r}} \qquad \Lambda = \frac{R_f + R_s}{k_{f,r}TCR\ A} \qquad Bi_s = \frac{L}{Rk_s} \qquad Bi_s = \frac{L}{Rk_{f,r}}$$

$$g_i(Fo) = \begin{cases} \dfrac{H_{ads}}{c_{p,s}(T_0 - T_{HTF})}\dfrac{d\omega}{dFo}, & i = s \\ 0, & i = f \end{cases}$$

where, θ_i is the dimensionless temperature of the i^{th} layer, Fo (Fourier number) is the dimensionless time, η and ξ are the dimensionless coordinates, and g_i is the dimensionless heat generation inside the i^{th} layer. Using the aforementioned dimensionless variables, the dimensionless energy equation as well as the boundary and initial conditions can be obtained:

$$\frac{\partial \theta_i}{\partial Fo} = (\mu_{i,\eta}\delta)^2\left(\frac{\partial^2\theta_i}{\partial\eta^2} + \frac{1}{\eta}\frac{\partial\theta_i}{\partial\eta}\right) + \mu_{i,\xi}{}^2\left(\frac{\partial^2\theta_i}{\partial\xi^2}\right) + g_i(Fo) \tag{12}$$

$$\frac{\partial\theta_i(\eta,1,Fo)}{\partial\xi} = 0 \tag{13}$$

$$\frac{\partial\theta_s(1,\xi,Fo)}{\partial\eta} = 0 \tag{14}$$

$$\frac{\partial\theta_f(0,\xi,Fo)}{\partial\eta} = 0 \tag{15}$$

$$\frac{\partial\theta_s(\eta,0,Fo)}{\partial\xi} - Bi_s\theta_s(\eta,0,Fo) = 0\frac{\partial\theta_f(\eta,0,Fo)}{\partial\xi} - Bi_f\theta_f(\eta,0,Fo) = 0 \tag{16}$$

$$\begin{aligned} \frac{\partial\theta_f(\delta_f,\xi,Fo)}{\partial\eta} &= \kappa\frac{\partial\theta_s(\delta_f,\xi,Fo)}{\partial\eta} - \frac{\partial\theta_f(\delta_f,\xi,Fo)}{\partial\eta} \\ &= \Lambda(\theta_f(\delta_f,\xi,Fo) - \theta_s(\delta_f,\xi,Fo)) \end{aligned} \tag{17}$$

A MATLAB code is developed to calculate the eigenfunctions and eigenvalues in both spatial coordinates along with the Gamma function as a function of Fourier number (dimensionless time). After solving the equations, the dimensionless temperature is acquired:

$$\theta(\eta,\xi,Fo) = \sum_{n=1}^{\infty}\sum_{m=1}^{\infty}\psi_n(\xi)\,\chi_{nm}(\eta)\,\Gamma_{nm}(Fo) \tag{18}$$

The methodology of the solution is presented in Appendix A.

Fig. 2. PF-HMX coated with the composite sorbent, silica gel, $CaCl_2$, PVA, and graphite flakes.

4. Experimental study

A number of $CaCl_2$-silica gel composite sorbents with 0-20 wt.% graphite flake contents is prepared. Polyvinyl alcohol (PVA) binder (40,000 MW, Amresco Inc.) is dissolved in water. Following this, $CaCl_2$ and silica gel (SiliaFlash® B150, Silicycle, Inc., Quebec, Canada) and graphite flakes (consisting of 150 μm fine particles and thin flakes up to 1.3 mm long, Sigma-Aldrich) are added to the aqueous solution. The slurry composites a coated on the designed PF-HMX and oven-dried at 70°C, then cured at 180°C, each for 4 hours, see Fig. 2 for more details. Thermophysical characteristics of the heat exchanger and sorbent materials with different amount of additives were measured using a transient plane source (TPS), hot disk thermal constants analyzer, as per ISO 22007- 2 (ISO220 07-2, 20 08) (TPS 250 0S, ThermTest Inc., Frederiction, Canada) and described in Table 2 (Fayazmanesh and Bahrami, 2017, Bahrehmand et al., 2018). Sorbent thickness around each fin and fin diameters are measured as 5 mm and 4 mm, respectively. Fig. 3 shows the diagram of the gravimetric large temperature jump (G-LTJ) testbed custom-built in our lab used to validate the developed analytical solution.

To simulate the operation of SCHS, HTF was pumped through the PF-HMX, and the temperature cycled between 30°C and 67°C for sorption and desorption, respectively. Two four-way valves were used to switch the HTF between the sorber bed and the buffer for desorption and sorption processes. The buffer was used for heat recovery purpose. The sorber bed and the copper PF-HMX were placed inside a vacuum chamber, which was connected to the evaporator/condenser that was maintained at 15°C. The whole testbed was degassed for five hours using a vacuum pump to dry the sorbent material before the tests. The vacuum chamber was placed on a precision balance (ML4002E, Mettler Toledo) with an accuracy of 0.01 g to measure the mass change due to the sorbate uptake. Five K-type thermocouples with an accuracy of 1.1°C were passed using a feed-through in the vacuum chamber to measure the sorbent temperature. The instruments were connected to a PC through a data acquisition system and in-house software written in a LabVIEW environment. The maximum uncertainties of the measured COP and SCP

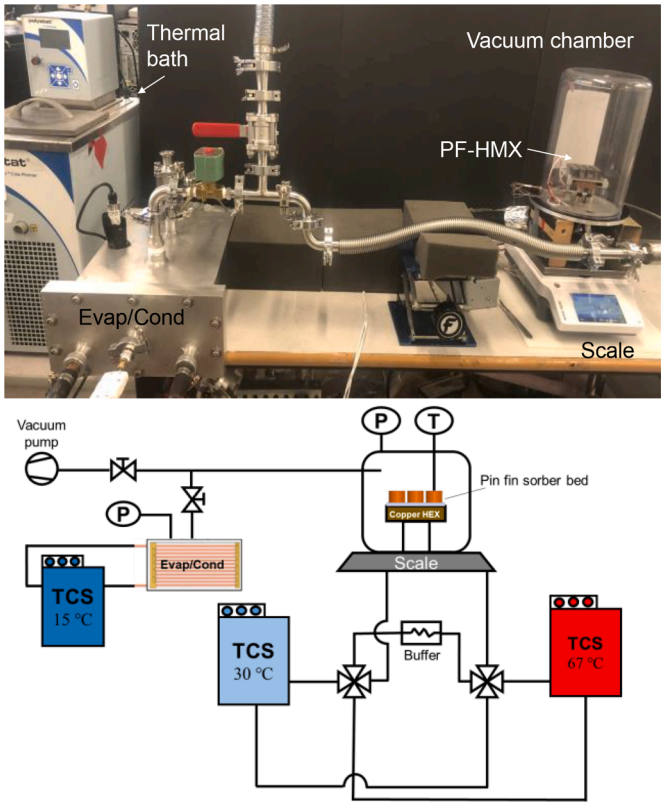

Fig. 3. A picture and a schematic diagram of the G-LTJ testbed.

Table 2
A summary of the Graphite flake content in the sorbent, thermophysical properties, geometrical specifications, and SCHS cycle parameters used for the baseline case and model validation.

	Baseline case			Validation with G-Ltestbedbed		
	Sorbent	Al fin	Al tube	Sorbent	Al fin	Copper tube
φ (wt%)	10	-	-	0-20		
ρ (kg m^{-3})	665	2699	2699		2699	8932
c (J kg^{-1} K^{-1})	1082	909	909		909	386
α (m^2 s^{-1})	4.1e-7	9.6e-5	9.6e-5		9.6e-5	1.1e-4
h_{ads} (J kg^{-1})	2.77e6	-	-	2.77e6		1.5
R_f, Δ_s, Δ_{HMX} (mm)	$\Delta_s = 2$	$R_f = 2$		$\Delta_s = 5$	$R_f = 2$	
L, H_c, W_c (cm)	L=2	L=1.5	H_c=0.6, W_c=1.3	L=1.5	L=1.5	H_c=0.5, W_c=4
t (min)	15			In Fig. 6		
$TCR.A$(K m^2 W^{-1})	0.0019 (Bahrehmand et al., 2018)					

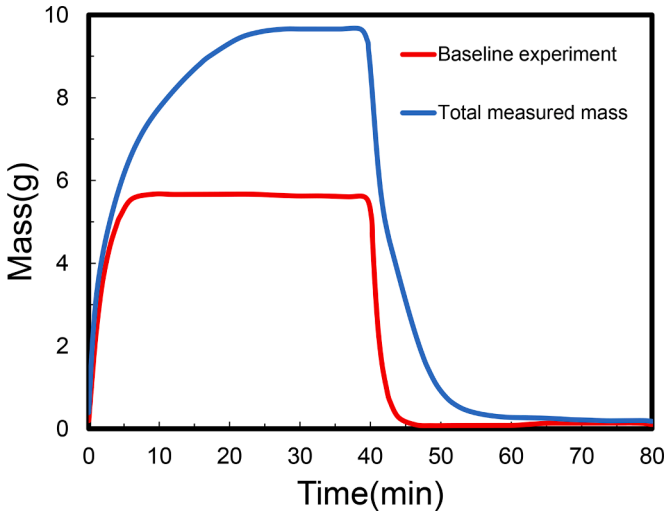

Fig. 4. Mass changes of the sorber bed with 0% graphite flake content in the G-LTJ testbed due to the variations in water density and fluctuations during the sorption (30 °C) and desorption (67 °C).

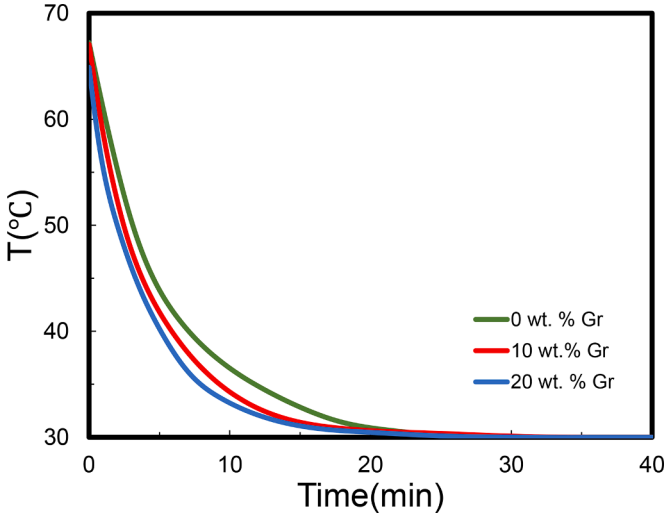

Fig. 5. Variation of average sorbent temperature through the time for a different amount of graphite flakes.

were estimated to be 8% and 5.7%, respectively. More information on uncertainty analysis can be found elsewhere (Bahrehmand et al., 2018).

5. Model validation

Figure 4 shows the mass change of the sorber bed for the sample with 0 % amount of graphite flakes. Measured mass change of the sorber bed is due to: (i) the water uptake by sorbent material, (ii) fluctuations such as thermal expansion, contraction, and vibration of the flexible hoses, and (iii) density changes of the heat transfer fluid (HTF) due to the temperature swings between adsorption and desorption processes. In order to deconvolute the mass change caused by the water uptake from others, a number of baseline experiments were run under the same operating conditions but with the valve between the sorber bed and the evaporator/condenser kept shut. Consequently, baseline did not include the effect of water uptake. After measuring the baseline signal, the valve was opened and the experiment was repeated; the blue line shows the total mass change of the sorber bed, including water uptake. Subtracting the total mass from the baseline represents the actual water uptake changes.

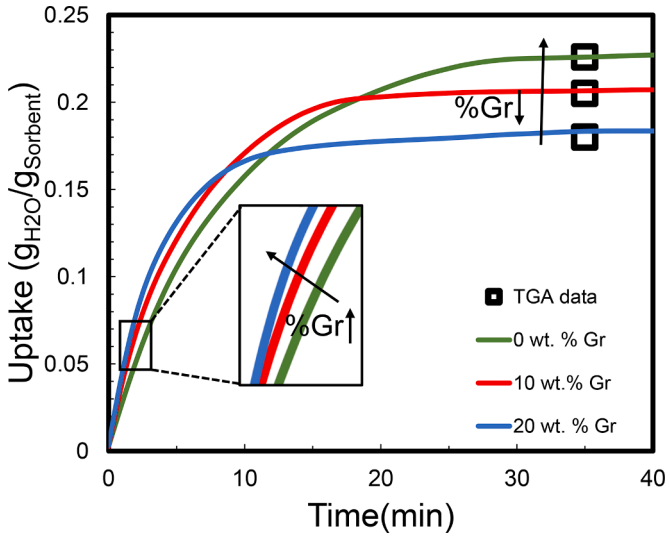

Fig. 6. Effect of graphite flake content on water uptake.

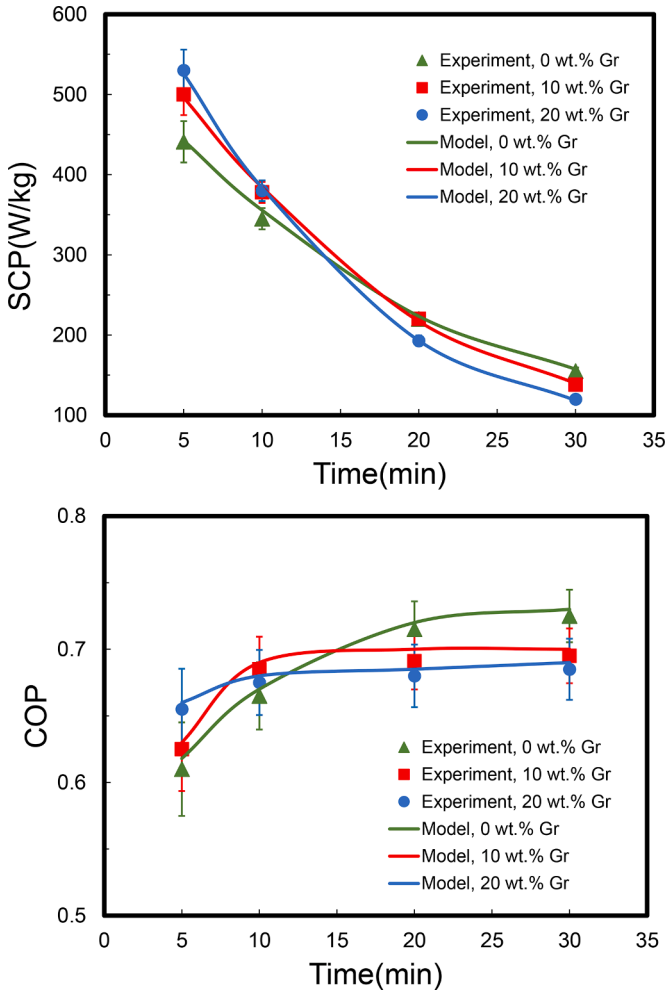

Fig. 7. Comparison between the present analytical model and the experimental data collected from our G-LTJ test bed for 0 and 20 wt% graphite flake content in the sorbent composite.

Figure 5 shows the variation of average sorbent temperature versus time for varying amounts of graphite flakes. By adding graphite flake, the sorbent thermal diffusivity improves up to 500% (Bahrehmand et al.,

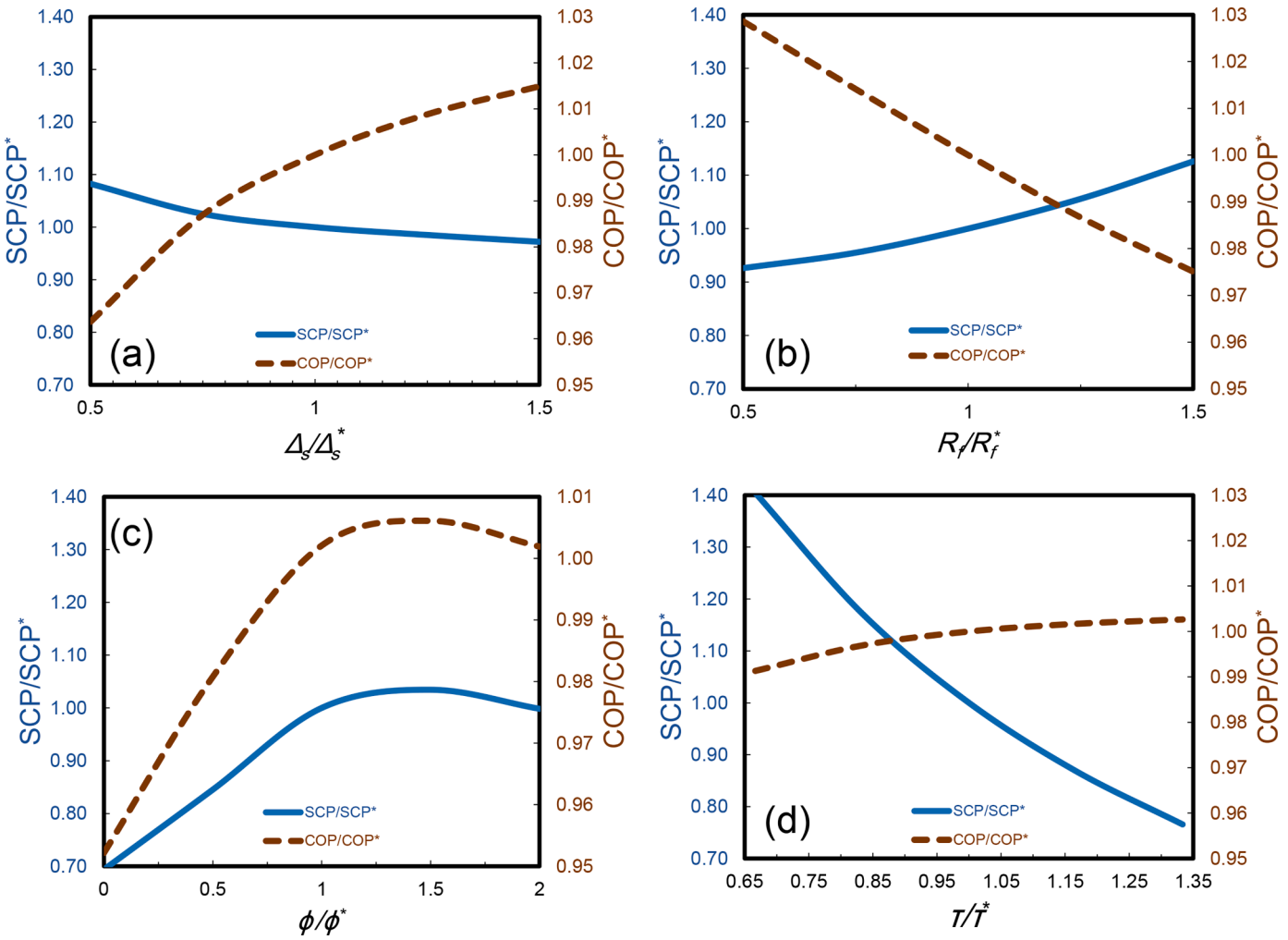

Fig. 8. Parametric study: COP and SCP Variation with sorber bed's geometry, heat transfer characteristics and cycle time (a) sorbent thickness, (b) fin radius, (c) graphite flake content in the sorbent, (d), cycle time. SCP* and COP* are the baseline values shown in Table 2.

2018), which enhances the heat transfer from HMX to the sorbent. For samples with higher amounts of graphite flakes and lower amounts of active material, the heat of sorption decreases.

Figure 6 shows the variation of the water uptake versus time for varying amounts of graphite flakes in the sorbent. In the early stage of sorption (the first 10 to 15 minutes), adding graphite flakes enhances water uptake. As the sorbent approaches saturation, the heat generation rate reduces and the trend starts to reverse. Moreover, a greater amount of graphite flake reduces the amount of active material, leading to lower uptake and performance as the sorbent reaches equilibrium. The equilibrium uptakes measured with the G-LTJ testbed are in good agreement with thermogravimetric sorption analyzer (TGA) equilibrium data; for more information, see (Bahrehmand et al., 2018).

Figure 7 shows the effect of graphite flakes on the SCP and COP based on Eqs. (1) and (2). It can be seen that the present analytical model is in good agreement with the experimental results. Moreover, for small sorption times (the first 10 to 15 minutes), SCP increases 10 to 30% by adding graphite flakes. Thus, during the early stages of sorption, the sorption rate and heat generation are high, resulting in a need for higher thermal diffusivity which in turn causes higher uptake. However, over longer periods of time, such as when the sorbent approaches saturation, the need for higher thermal diffusivity reduces as the sorption rate decreases. The trend starts to reverse and the sorbent with higher active material has higher uptake and higher SCP.

Additionally, for a small sorption time, the sample with higher graphite flakes has higher uptake and thus higher COP. As we approach the saturation phase, the sample with a smaller amount of additives and a greater amount of active material has the highest uptake and COP.

6. Results and discussion

6.1. Parametric Study

A comprehensive parametric study is carried out to examine the effect of key design and operating variables on the COP and SCP, namely, fin radius, sorbent thickness, graphite flake content in the sorbent, and the cycle time. Sorber bed characteristic parameters are considered as a baseline in which each parameter is changed over an arbitrarily chosen range while other parameters are kept constant. It should be noted that the results are particular to the values and conditions described in table 2 and might be different for other input parameters. SCP and COP for baseline condition listed in Table 2 are 737 W kg^{-1} K^{-1} and 0.66, respectively.

The following conclusions can be made from Fig. 8 (a-d):

- SCP decreases by the sorbent thickness increment because the sorbent heat transfer resistance enhances. However, COP increases by the sorbent thickness increment as the amount of active material increases;
- SCP increases by increasing the fin radius as the heat transfer along the fin enhances due to the larger cross-sectional area. Nonetheless,

Table 3
Three levels of the PF-HMX design parameters.

	Level 1	Level 2 (baseline case)	Level 3
Fin height (L (cm))	1	2	3
Fin radius (R_f (mm))	1	2	3
Sorbent thickness (Δ_s (mm))	1	2	3
Graphite flake content (φ (wt.%))	0	10	20
Fluid channel height (Hc (mm))	4	6	8
Cycle time (τ (min))	10	15	20

Table 4
The calculated p-value of all design parameters by MATLAB for the SCP and COP.

Parameters	COP	SCP
Fin height (L (cm))	4.78e-12	7.04e-8
Fin radius (R_f (mm))	5.73e-25	4.41e-16
Sorbent thickness (Δ_s (mm))	9.76e-28	6.66e-8
Graphite flake content (φ (wt. %))	8.11e-32	2.57e-28
Fluid channel height (H_c (mm))	5.14e-2	6.34e-2
Cycle time (τ (min))	3.72e-16	6.64e-36

COP decreases by increasing the fin radius because the dead weight mass (thermal inertia) is increased increases;

- Thermal diffusivity can be enhanced by additive material. Previous studies showed that the thermal diffusivity of the sorbent can be increased up to 500% by adding graphite flakes as an additive, although it will reduce the amount of active material (Bahrehmand et al., 2018). Therefore, it is important to select an optimum amount of additive, which depends on the geometry and heat transfer characteristics of a sorber bed. SCP and COP both increase by the graphite flake content increment to the point until it keeps up with heat transfer resistance in the fin. After the climax, SCP starts to decrease by increasing the graphite flake content as the active sorbent material decreases; and
- SCP increases by reducing the cycle time as the sorption rate is higher at the beginning of sorption and drops as the sorbent approaches saturation. Nevertheless, COP decreases slightly by reducing the cycle time as more energy needs to be provided for the sensible heat of the sorber bed HMX thermal inertia with respect to the desorption heat.

It is evident that geometry, sorbent properties, and cycle time can have counteracting effects on COP and SCP and should be optimized simultaneously to build an optimal design to be investigated in future studies. The following section is focused on an analysis of variance of the proposed PF-HMX to address the need for this simultaneous optimization.

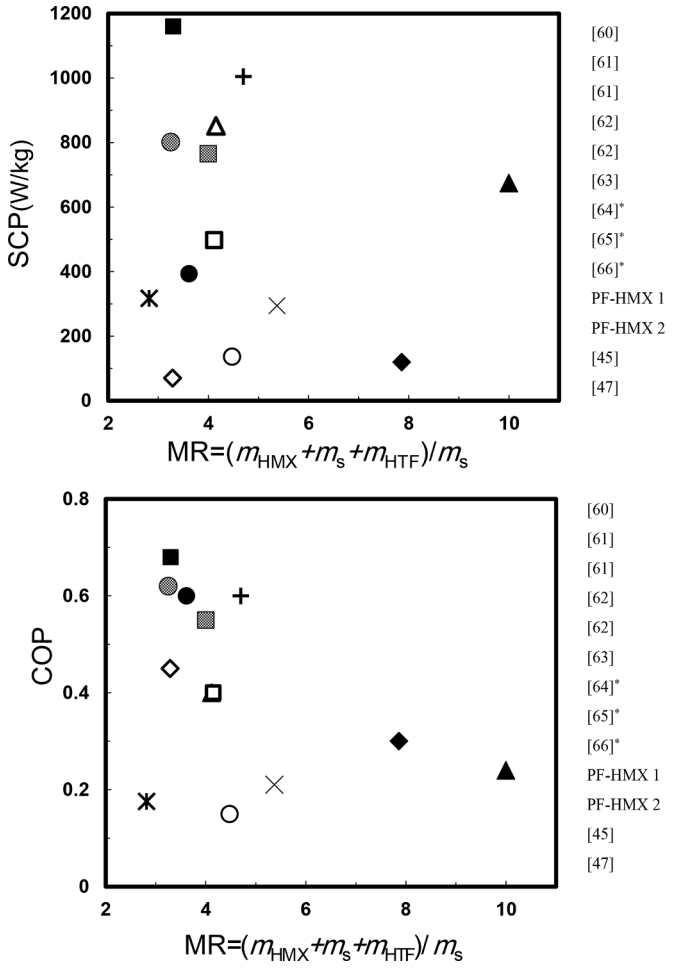

Fig. 10. PF-HMX comparison in terms of the MR, SCP, and COP versus the available studies. Fin radius and sorbent thickness of PF-HMX 1 are 2 mm and 5 mm, respectively, while fin radius and sorbent thickness for PF-HMX 2 are 1mm and 2 mm respectively. * HTF data not provided.

6.2. Analysis of variance (ANOVA)

The ANOVA method is utilized to understand the percentage contribution of each parameter on SCP and COP (Asghar et al., 2014). A Multi-way ANOVA analysis is performed using the NANOVA function in MATLAB; for further details, see (Bahrehmand and Bahrami, 2020). Table 3 shows the sample points of variables generated using the Box-Behnken design (Box and Behnken, 1960) with three levels of design parameters.

The null hypothesis is used to see whether a variable has a substantial

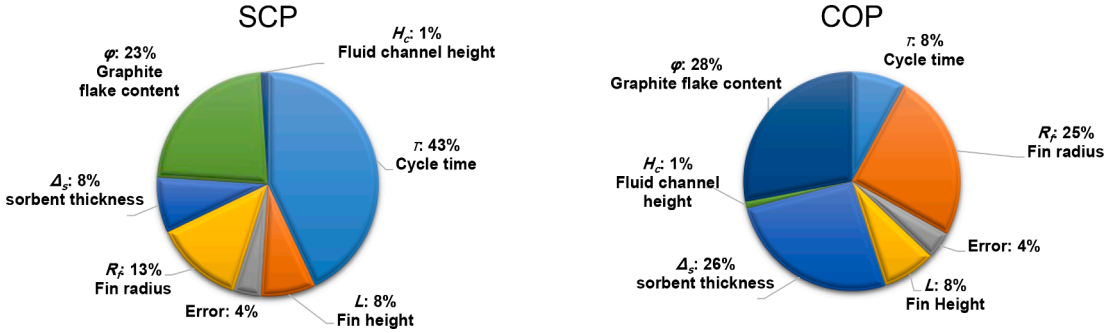

Fig. 9. The level of contribution of design parameters to the SCP and COP, L: fin height, R_f: fin radius, Δ_s: sorbent thickness, φ: graphite flake content in the sorbent, t: cycle time, H_C: fluid channel height.

effect on the objective function. When α is greater than the p-value, then the null hypothesis is rejected. α is the significance level and it is usually equal to 0.05 which means there is a 5% probability that the null hypothesis was incorrect and the parameter has a significant effect. The p-value also can be estimated by MATLAB as a function of the F-static ratio, α, and degree of freedom.

We found that all p-values, shown in Table 4, are less than α except the p-value for the heat transfer fluid channel height which is greater than α. Therefore, all factors are affecting the responses except the heat transfer fluid channel height that should be considered as a parameter as its share in the objective functions is negligible.

The results of this analysis for both COP and SCP are shown in Fig. 9 and represent how all these parameters affect the COP and SCP of the system. As can be seen, the amount of graphite flake, sorbent thickness, and fin radius on one hand and cycle time and graphite flake content on the other have the highest level of contribution to the COP and SCP, respectively.

6.3. Performance evaluation

The baseline case is investigated for the operating conditions of the sorption chiller: T_{des}=90°C, T_{ads}=T_{cond}=30°C, and T_{evap}=15°C. SCP, COP, and MR are calculated as performance metrics based on equations. (1), (2), and (3). Note that the mass of heat transfer fluid was not available for some studies. The PF-HMX with relatively low MR reaches a SCP of 1160 W kg^{-1} and COP of 0.68. Fig. 10 displays the performance of PF-HMX versus state-of-the-art published researches. Note that the composite silica gel/$CaCl_2$ sorbent used in the PF-HMX, (Bahrehmand and Bahrami, 2019) and (Bahrehmand and Bahrami, 2020) provide higher SCP and COP. Silica gel/CaCl2 sorption kinematic occurs over the entire range of relative pressure $0.06<P/P_0<0.4$ which makes it a good candidate for AC applications (Bahrehmand et al., 2018). Conversely, sorption for zeolite-based materials, such as SAPO-34 and FAM Z02, utilized in (Sapienza et al., 2011, Freni et al., 2015, Sharafian, 2016, Wittstadt et al., 2017, Freni, 2007, Dawoud et al., 2010, Aristov et al., 2010) occurs in a narrow range of relative pressure which limits the application to specific operational temperatures.

7. Summary and conclusions

A novel closed-form 2-D analytical model was developed to determine the conjugate heat and mass transfer and performance of PF-HMX. The analytical solution included material properties, operating conditions and all design parameters such as sorbent geometry, HMX geometry, and fluid channel height. The current 2-D model was successfully validated based on experimental results collected from a custom-built G-LTJ testbed.

Additionally, based on the parametric study and ANOVA, it was shown that the heat transfer and geometrical characteristics of sorber bed, such as sorbent thickness, fin radius, fin height, amount of graphite flakes, cycle time, and fluid channel height, have conflicting effects on COP and SCP. Thus, a multi-objective optimization procedure should be conducted to find an optimal design of the sorber bed for future studies based on geometrical and heat transfer characteristics of the sorber bed. To this end, we compared two arbitrary geometries of PF-HMX with other studies and found that PF-HMX with a relatively low MR could provide high SCP and COP.

Declaration of Competing Interest

The authors declare that they have no known competing financial interests or personal relationships that could have appeared to influence the work reported in this paper.

Acknowledgment

The authors gratefully acknowledge the financial support of the Natural Sciences and Engineering Research Council of Canada (NSERC) through the Advancing Climate Change Science in Canada (ACCSC) Grant No. ACCPJ 536076-18

Appendix A

Dimensionless energy equation obtained as (9) where

$$\mu_{i,\eta} = \begin{cases} \mu_r, & i = f \\ \mu_s, & i = s \end{cases} \tag{A.1}$$

$$\mu_{i,\xi} = \begin{cases} 1, & i = f \\ \mu_s, & i = s \end{cases} \tag{A.2}$$

Water uptake can be simulated as a function of operating conditions such as pressure and temperature of sorber bed. A linear relationship between water uptake and sorbent temperature is achieved by (Bahrehmand et al., 2018, Bahrehmand et al., 2018) for each pressure during isobaric desorption and adsorption processes.

$$\omega_{des} = -0.0123\ T + 4.0106 \tag{A.3}$$

$$\omega_{ads} = -0.0118\ T + 3.9852 \tag{A.4}$$

The Eigenfunction expansion method is used to solve the dimensionless energy equation and boundary conditions, Eqs. (12)-(17) and find the closed-form relationship of dimensionless temperature as follows:

$$\theta(\eta, \xi, Fo) = \sum_{n=1}^{\infty} \sum_{m=1}^{\infty} \psi_n(\xi)\ \chi_{nm}(\eta)\ \Gamma_{nm}(Fo) \tag{A.5}$$

Based on Eqs. (12)-(17) and (A.5), the following eigenvalue problem can be derived in ξ direction (Soloukhin and Martynenko, 1985, Mikhailov and Özişik, 1986).

$$\psi'' + \gamma^2 \psi = 0 \tag{A.6}$$

$$\psi' + Bi\ \psi = 0\ at\ \xi = 0 \tag{A.7}$$

$$\psi = 0\ at\ \xi = 0 \tag{A.8}$$

The following transcendental equation is achieved to calculate the eigenvalues.

$$\gamma \tan\gamma = Bi \tag{A.9}$$

The eigenfunction related to each eigenvalue is given as follows.

$$\psi = \cos(\gamma\xi) + \tan(\gamma)\sin(\gamma\xi) \tag{A.10}$$

Furthermore, the following eigenvalue problem can be established in the η direction.

$$\frac{d^2\chi}{d\eta^2} + \frac{1}{\eta}\frac{d\chi}{d\eta} + \omega_k^2\chi = 0 \tag{A.11}$$

$$\frac{d\chi}{d\eta} = 0 \ at \ \eta = 0, 1 \tag{A.12}$$

where,

$$\omega_k^2 = \frac{\lambda r_k - q_k}{p_k}, \ k = s,f \tag{A.13}$$

$$r_s = \frac{\left((\rho c_p) - \left(\rho H_{ads}\ \omega_{ads/des}\right)_s\right)k_z}{(\rho c_p)_f \delta^2} \tag{A.14}$$

$$r_f = \frac{k_{f,z}}{\delta^2} \tag{A.15}$$

$$q_k = \left(\mu_{k,\eta}\gamma\right)^2 r_k \tag{A.16}$$

$$p_f = k_{f,r} \tag{A.17}$$

$$p_s = k_s \tag{A.18}$$

This is a singular eigenvalue problem because of non-continuous *p, r,* and *q*. Further, ω^2_k, depending upon the thermophysical properties and geometrical characteristics of the sorbent and the fin, can be positive, negative, or zero. Therefore, there is no simple solution with eigenfunction and transcendental equation for the eigenvalue problem. The approximated solution proposed by (Soloukhin and Martynenko, 1985, Mikhailov and Vulchanov, 1983) is followed in the present paper. The eigenvalue problem is approximated by identically diving the cylinder (sorbent and fin) into *n*-1 intervals. The finer the division, the better the approximation. The following equations represent the new eigenvalue problem with boundary conditions.

$$\frac{d^2\chi}{d\eta^2} + \frac{1}{\eta}\frac{d\chi}{d\eta} + \omega_k^2\chi = 0 \tag{A.19}$$

$$\frac{d\chi}{d\eta} = 0 \ at \ \eta = 0 \tag{A.20}$$

$$\chi_k = \chi_{k+1}\ , \ k = 2, 3, .., n-1 \tag{A.21}$$

$$p_k\frac{d\chi_k}{d\eta} = p_{k+1}\frac{d\chi_{k+1}}{d\eta}, \ k = 2, 3, .., n-1 \tag{A.22}$$

$$\frac{d\chi}{d\eta} = 0 \ at \ \eta = 1 \tag{A.23}$$

The following equations are also established to consider TCR as an imaginary layer at the interface between sorbent and the fin.

$$\frac{d^2\chi}{d\eta^2} + \frac{1}{\eta}\frac{d\chi}{d\eta} + \omega_k^2\chi = 0 \tag{A.24}$$

$$\omega_k = 0 \tag{A.25}$$

$$p_k\frac{d\chi}{d\eta} = \frac{R_f + \Delta_s}{TCR.A}(\chi_{k+1} - \chi_k) \tag{A.26}$$

The following eigenfunction can be achieved for each interval ($\xi_{k\text{-}1}<\xi<\xi_k$).

$$\chi_k(\eta) = \chi_k(\eta_{k-1})\frac{J_0(\omega_k\eta)Y_0(\omega_k\eta_k) - J_0(\omega_k\eta_k)Y_0(\omega_k\eta)}{J_0(\omega_k\eta_{k-1})Y_0(\omega_k\eta_k) - J_0(\omega_k\eta_k)Y_0(\omega_k\eta_{k-1})} + \chi_k(\eta_k)\frac{J_0(\omega_k\eta_{k-1})Y_0(\omega_k\eta) - J_0(\omega_k\eta)Y_0(\omega_k\eta_{k-1})}{J_0(\omega_k\eta_{k-1})Y_0(\omega_k\eta_k) - J_0(\omega_k\eta_k)Y_0(\omega_k\eta_{k-1})}, \ \omega_k^2 > 0 \tag{A.27}$$

$$\chi_k(\eta) = \chi_k(\eta_{k-1})Log^{\frac{\eta}{\eta_k}}_{\frac{\eta_{k-1}}{\eta_k}} + \chi_k(\eta_k)Log^{\frac{\eta_{k-1}}{\eta}}_{\frac{\eta_{k-1}}{\eta_k}}, \ \omega_k^2 = 0 \tag{A.28}$$

$$\chi_k(\eta) = \chi_k(\eta_{k-1})\frac{I_0(\omega_k^*\eta)K_0(\omega_k^*\eta_k) - I_0(\omega_k^*\eta_k)K_0(\omega_k^*\eta)}{I_0(\omega_k^*\eta_{k-1})K_0(\omega_k^*\eta_k) - I_0(\omega_k^*\eta_k)K_0(\omega_k^*\eta_{k-1})} + \chi_k(\eta_k)\frac{I_0(\omega_k^*\eta_{k-1})K_0(\omega_k^*\eta) - I_0(\omega_k^*\eta)K_0(\omega_k^*\eta_{k-1})}{I_0(\omega_k^*\eta_{k-1})K_0(\omega_k^*\eta_k) - I_0(\omega_k^*\eta_k)K_0(\omega_k^*\eta_{k-1})}, \ \omega_k^2 < 0 \tag{A.29}$$

$$\omega_k^* = \sqrt{abs(\omega_k^2)} \tag{A.30}$$

The Eigenfunctions for each interval can be calculated as follows by substituting the abovementioned eigenfunctions into boundary conditions ((A.20)-(A.23)).

$$A_1\chi_0 - B_1\chi_1 = 0 \tag{A.31}$$

$$B_k\chi_{k-1} + (A_k + A_{k+1})\chi_k - B_{k+1}\chi_{k+1} = 0\ ,\ k = 2, \ldots, n-1 \tag{A.32}$$

$$-B_n\chi_{n-1} + A_n\chi_n = 0 \tag{A.33}$$

where,

$$A_k = p_k\omega_k\left(\frac{J_0(\omega_k\eta_k)Y_1(\omega_k\eta_k) - Y_0(\omega_k\eta_k)J_1(\omega_k\eta_{k-1})}{J_0(\omega_k\eta_{k-1})Y_0(\omega_k\eta_k) - J_0(\omega_k\eta_k)Y_0(\omega_k\eta_{k-1})}\right),\ \omega_k^2 > 0 \tag{A.34}$$

$$A_k = 1\ ,\omega_k^2 = 0 \tag{A.35}$$

$$A_k = p_k\omega_k\left(\frac{I_0(\omega_k^*\eta_k)K_1(\omega_k^*\eta_k) - K_0(\omega_k^*\eta_k)I_1(\omega_k^*\eta_{k-1})}{I_0(\omega_k^*\eta_{k-1})K_0(\omega_k^*\eta_k) - I_0(\omega_k^*\eta_k)K_0(\omega_k^*\eta_{k-1})}\right),\ \omega_k^2 < 0 \tag{A.36}$$

$$B_k = p_k\omega_k\left(\frac{J_0(\omega_k\eta_{k-1})Y_1(\omega_k\eta_{k-1}) - Y_0(\omega_k\eta_{k-1})J_1(\omega_k\eta_{k-1})}{J_0(\omega_k\eta_{k-1})Y_0(\omega_k\eta_k) - J_0(\omega_k\eta_k)Y_0(\omega_k\eta_{k-1})}\right),\ \omega_k^2 > 0 \tag{A.37}$$

$$B_k = 1\ ,\omega_k^2 = 0 \tag{A.38}$$

$$B_k = p_k\omega_k\left(\frac{I_0(\omega_k^*\eta_{k-1})K_1(\omega_k^*\eta_{k-1}) - K_0(\omega_k^*\eta_{k-1})I_1(\omega_k^*\eta_{k-1})}{I_0(\omega_k^*\eta_{k-1})K_0(\omega_k^*\eta_k) - I_0(\omega_k^*\eta_k)K_0(\omega_k^*\eta_{k-1})}\right)\ \omega_k^2 < 0 \tag{A.39}$$

A linear system of homogenous equations formed based on Eqs. (A.31)-(A.33) is derived as follows in order to calculate the eigenfunctions.

$$[K]\ \{\chi\} = 0 \tag{A.40}$$

The transcendental equation is obtained to calculate the eigenvalues by equating the determinant of coefficient matrix $[K]$ to zero.

$$det([K]) = 0 \tag{A.41}$$

The sign-count method, developed by Mikhailov and Vulchanov, is utilized to solve the transcendental equation (Soloukhin and Martynenko, 1985).

Eventually, eigenfunction is evaluated as follows.

$$\chi_0 = -1 \tag{A.42}$$

$$\chi_1 = -\frac{A_1}{B_1} \tag{A.43}$$

$$\chi_{k+1} = \frac{((A_k + A_{k+1})\chi_k - B_k\chi_{k-1})}{B_{k+1}}\ ,\ k = 1, 2, \ldots, n-1 \tag{A.44}$$

Subsequently, the accuracy of the eigenfunction is evaluated for the last interval. If the required accuracy, 1e-8 for this study, is not satisfied, then the finer intervals will be chosen based on the algorithm proposed by (Mikhailov and Vulchanov, 1983) until it is satisfied.

$$|-B_n\chi_{n-1} + A_n\chi_n| \le \varepsilon_{global},\ \varepsilon_{global} \cong \varepsilon_{max}.n \tag{A.45}$$

To this end, the eigenfunctions in ξ and η directions are evaluated. The last step is to acquire the Gamma function. Gamma function, which shows the time variation of θ, can be expanded in the form of infinite series of products of eigenfunctions in ξ and η directions as follows.

$$g_i(Fo) = \sum_{n=1}^{\infty}\sum_{m=1}^{\infty} g_{nm}^*(Fo)\psi_n(\xi)\,\chi_{nm}(\eta) \tag{A.46}$$

where, g^*_{nm} can be calculated based on the orthogonal property of the eigenfunctions as follows.

$$g_{nm}^*(Fo) = \frac{g_i(Fo)\int_0^1 \psi d\xi\left(\sum_{k=1}^n r_k \int_{\eta_k}^{\eta_{k+1}} \chi_k d\eta\right)}{\int_0^1 \psi^2 d\xi\left(\sum_{k=1}^n r_k \int_{\eta_k}^{\eta_{k+1}} {\chi_k}^2 d\eta\right)} \tag{A.47}$$

By substituting Eqs. (A.5) and (A.46) into Eq. (12), the following ordinary differential equation can be obtained for the Gamma function.

$$\frac{d\Gamma}{dFo} = g_{nm}^*(Fo) - \lambda\Gamma \tag{A.48}$$

Finally, the Gamma function is evaluated as follows.

$$\Gamma = e^{-\lambda Fo}\left(C_{nm} + \int_{Fo'=0}^{Fo} g_{nm}^{*}(Fo')e^{\lambda Fo'}dFo'\right) \tag{A.49}$$

where,

$$C_{nm} = \frac{\int_0^1 \psi d\xi\left(\sum_{k=1}^{n} r_k \int_{\eta_k}^{n_{k+1}} \chi_k d\eta\right)}{\int_0^1 \psi^2 d\xi\left(\sum_{k=1}^{n} r_k \int_{\eta_k}^{n_{k+1}} {\chi_k}^2 d\eta\right)} \tag{A.50}$$

References

Ürge-Vorsatz, D., Cabeza, L.F., Serrano, S., Barreneche, C., Petrichenko, K., 2015. Heating and cooling energy trends and drivers in buildings. Renew. Sustain. Energy Rev. 41, 85–98.

Askalany, A.A., Salem, M., Ismael, I.M., Ali, A.H.H., Morsy, M.G., Saha, B.B., 2013. An overview on adsorption pairs for cooling. Renew. Sustain. Energy Rev. 19, 565–572.

Pridasawas, W., 2006. Solar-driven refrigeration systems with focus on the ejector cycle. Department of Energy Technology, Royal Institute of Technology, p. 2006 no. 06/55.

Cullen, J.M., Ã, J.M.A., 2010. The efficient use of energy : Tracing the global flow of energy from fuel to service. Energy Policy 38 (1), 75–81.

Pinheiro, J.M., Salústio, S., Rocha, J., Valente, A.A., Silva, C.M., 2016. Analysis of equilibrium and kinetic parameters of water adsorption heating systems for different porous metal/metalloid oxide adsorbents. Appl. Therm. Eng. 100, 215–226.

Demir, H., Mobedi, M., Ülkü, S., 2008. A review on adsorption heat pump: Problems and solutions. Renew. Sustain. Energy Rev. 12 (9), 2381–2403.

Forman, C., Muritala, I.K., Pardemann, R., Meyer, B., 2016. Estimating the global waste heat potential. Renew. Sustain. Energy Rev. 57, 1568–1579.

Zhao, Y., Hu, E., Blazewicz, A., 2012. Dynamic modelling of an activated carbon–methanol adsorption refrigeration tube with considerations of interfacial convection and transient pressure process. Appl. Energy 95, 276–284.

Wu, W.D., Zhang, H., Sun, D.W., 2009. Mathematical simulation and experimental study of a modified zeolite 13X-water adsorption refrigeration module. Appl. Therm. Eng. 29 (4), 645–651.

A. Sharafian, S. M. N. Mehr, P. C. Thimmaiah, W. Huttema, and M. %J E. Bahrami, "Effects of adsorbent mass and number of adsorber beds on the performance of a waste heat-driven adsorption cooling system for vehicle air conditioning applications," vol. 112, pp. 481–493, 2016.

Hu, E.J., Zhu, D., Sang, X., Wang, L., Tan, Y., 1997. Enhancement of Thermal Conductivity by Using Polymer- Zeolite in Solid Adsorption Heat Pumps. J. Heat Transfer 1 (August), 1991–1993.

Saha, B.B., Koyama, S., El-Sharkawy, I.I., Kuwahara, K., Kariya, K., Ng, K.C., 2006. Experiments for measuring adsorption characteristics of an activated carbon fiber/ethanol pair using a plate-fin heat exchanger. HVAC R Res 12 (September 2014), 767–782.

Henninger, S., Schicktanz, M., Hugenell, P., S, H., Henning, H., 2012. Evaluation of methanol adsorption on activated carbons for thermally driven chillers, part I: thermophysical characterisation. Int J Refrig 35, 543–553.

Tamainot-Telto, Z., Metcalf, S.J., Critoph, R.E., Zhong, Y., Thorpe, R., 2009. Carbon – ammonia pairs for adsorption refrigeration applications : ice making, air conditioning and heat pumping Les couples charbon actif-ammoniac pour les applications ` adsorption : fabrication de glace, frigorifiques a ` chaleur conditionnement d '. Int. J. Refrig. 32 (6), 1212–1229.

Saha, B., El-Sharkawy, I., Chakraborty, A., Koyama, S., 2007. Study on an activated carbon fiber-ethanol adsorption chiller: part I – system description and modelling. Int J Refrig 30, 86–95.

Pan, Q.W., Wang, R.Z., Wang, L.W., Liu, D., 2016. Design and experimental study of a silica gel-water adsorption chiller with modular adsorbers. Int. J. Refrig. 67, 336–344.

Ahmed, R., Al-Dadah, R., 2012. Physical and operating conditions effects on silica gel/water adsorption chiller performance. Appl Energy 89, 142–149.

Rogala, Z., 2017. Adsorption chiller using flat-tube adsorbers – Performance assessment and optimization. Appl. Therm. Eng. 121, 431–442.

Mitra, S., Muttakin, M., Thu, K., Saha, B.B., 2018. Study on the influence of adsorbent particle size and heat exchanger aspect ratio on dynamic adsorption characteristics. Appl. Therm. Eng. 133, 764–773.

Guilleminot, J.J., Meunier, F., Pakleza, J., 1987. Heat and mass transfer in a non-isothermal fixed bed solid adsorbent reactor: a uniform pressure-non-uniform temperature case. Int. J. Heat Mass Transf. 30 (8), 1595–1606.

Jribi, S., Miyazaki, T., Saha, B.B., Koyama, S., Maeda, S., Maruyama, T., 2017. Simulation par la mécanique numérique des fluides (CFD) et validation expérimentale de l'adsorption de l'éthanol sur un échangeur de chaleur compact à charbon actif. Int. J. Refrig. 74, 343–351.

Alam, K.C.A., Saha, B.B., Kang, Y.T., Akisawa, A., Kashiwagi, T., 2000. Heat exchanger design effect on the system performance of silica gel adsorption refrigeration systems. Int. J. Heat Mass Transf. 43 (24), 4419–4431.

Amini, H., Steen, S., 2012. Theoretical and experimental investigation of propeller. Int. Shipbuild. Prog. 59 (18), 55–82.

Amar, N.Ben, Sun, L.M., Meunier, F., 1996. Numerical analysis of adsorptive temperature wave regenerative heat pump. Appl. Therm. Eng. 16 (5), 405–418. SPEC. ISS.

Zhang, L.Z., Wang, L., 1999. Effects of coupled heat and mass transfers in adsorbent on the performance of a waste heat adsorption cooling unit. Appl. Therm. Eng. 19 (2), 195–215.

El Fadar, A., 2015. Thermal behavior and performance assessment of a solar adsorption cooling system with finned adsorber. Energy 83, 674–684.

Ndiaye, K., Ginestet, S., Cyr, M., 2017. Modelling and experimental study of low temperature energy storage reactor using cementitious material. Appl. Therm. Eng. 110, 601–615.

Duquesne, M., Toutain, J., Sempey, A., Ginestet, S., Palomo Del Barrio, E., 2014. Modeling of a nonlinear thermochemical energy storage by adsorption on zeolites. Appl. Therm. Eng. 71 (1), 469–480.

Solmus, I., et al., 2012. A two-energy equation model for dynamic heat and mass transfer in an adsorbent bed using silica gel/water pair. Int. J. Heat Mass Transf. 55, 5275–5288.

Li, J., Kubota, M., Watanabe, F., Kobayashi, N., Hasatani, M., 2004. Optimal Design of a Fin-type Silica Gel Tube Module in the Silica Gel /Water Adsorption Heat Pump. J. Chem. Eng. Japan 37 (4), 551–557.

Mhimid, A., 1998. Theoretical study of heat and mass transfer in a zeolite bed during water desorption: validity of local thermal equilibrium assumption. Int. J. Heat Mass Transf. 41 (19), 2967–2977.

Niazmand, H., Dabzadeh, I., 2012. Numerical simulation of heat and mass transfer in adsorbent beds with annular fins. Int. J. Refrig. 35 (3), 581–593.

Mohammed, R.H., Mesalhy, O., Elsayed, M.L., Chow, L.C., 2017. Conception d'un nouveau lit compact pour systèmes de refroidissement à adsorption: étude numérique paramétrique. Int. J. Refrig. 80, 238–251.

Tatsidjodoung, P., Pierrès, N.Le, Heintz, J., Lagre, D., Luo, L., Durier, F., 2016. Experimental and numerical investigations of a zeolite 13X/water reactor for solar heat storage in buildings. Energy Convers. Manag. 108, 488–500.

Golparvar, B., Niazmand, H., Sharafian, A., Hosseini, A.Ahmadian, 2018. Optimum fin spacing of finned tube adsorber bed heat exchangers in an exhaust gas-driven adsorption cooling system. Appl. Energy 232 (September), 504–516.

Passos, E.F., Escobedo, J.F., Meunier, F., 1989. Simulation of an intermittent adsorptive solar cooling system. Sol. Energy 42 (2), 103–111.

Mette, B., Kerskes, H., Drück, H., 2014. Experimental and numerical investigations of different reactor concepts for thermochemical energy storage. Energy Procedia 57, 2380–2389.

Aydin, D., Casey, S.P., Chen, X., Riffat, S., 2018. Numerical and experimental analysis of a novel heat pump driven sorption storage heater. Appl. Energy 211 (July 2017), 954–974.

Lele, A.F., Rönnebeck, T., Rohde, C., Schmidt, T., Kuznik, F., Ruck, W.K.L., 2014. Modelling of heat exchangers based on thermochemical material for solar heat storage systems. Energy Procedia 61, 2809–2813.

Bhouri, M., Bürger, I., 2017. Numerical investigation of H2 absorption in an adiabatic high-temperature metal hydride reactor based on thermochemical heat storage: MgH2 and Mg(OH)2 as reference materials. Int. J. Hydrogen Energy 42 (26), 16632–16644.

Fopah Lele, A., Kuznik, F., Rammelberg, H.U., Schmidt, T., Ruck, W.K.L., 2015. Thermal decomposition kinetic of salt hydrates for heat storage systems. Appl. Energy 154, 447–458.

Hong, S.W., Ahn, S.H., Kwon, O.K., Chung, J.D., 2015. Optimization of a fin-tube type adsorption chiller by design of experiment. Int. J. Refrig. 49, 49–56.

Çağlar, A., 2016. The effect of fin design parameters on the heat transfer enhancement in the adsorbent bed of a thermal wave cycle. Appl. Therm. Eng. 104, 386–393.

Bahrehmand, H., Ahmadi, M., Bahrami, M., 2018. Analytical modeling of oscillatory heat transfer in coated sorption beds. Int. J. Heat Mass Transf. 121, 1–9.

Bahrehmand, H., Bahrami, M., 2019. An analytical design tool for sorber bed heat exchangers of sorption cooling systems. Int. J. Refrig. 100, 368–379.

Jeric, M.Z., Nottage, H.B., 2012. Coupled Periodic Heat and Mass Transfer Through a Permeable Slab With Vapor Adsorption. J. Heat Transfer 89 (1), 44.

H. Bahrehmand and M. Bahrami, "Optimized sorber bed heat and mass exchangers for sorption cooling systems," no. October, 2020.

Demir, H., Mobedi, M., Ülkü, S., 2010. The use of metal piece additives to enhance heat transfer rate through an unconsolidated adsorbent bed. Int. J. Refrig. 33 (4), 714–720.

Rezk, A., Al-Dadah, R.K., Mahmoud, S., Elsayed, A., 2013. Effects of contact resistance and metal additives in finned-tube adsorbent beds on the performance of silica gel/water adsorption chiller. Appl. Therm. Eng. 53 (2), 278–284.

Gediz Ilis, G., Demir, H., Mobedi, M., Baran Saha, B., 2019. A New Adsorbent Bed Design: Optimization of Geometric Parameters and Metal Additive for the Performance Improvement. Appl. Therm. Eng. 162 (August), 114270.

Khatibi, M., Mohammadzadeh Kowsari, M., Golparvar, B., Niazmand, H., 2021. Optimum loading of aluminum additive particles in unconsolidated beds of finned flat-tube heat exchangers in an adsorption cooling system. Appl. Therm. Eng. 196 (June), 117267.

Bahrehmand, H., Ahmadi, M., Bahrami, M., 2018. Oscillatory heat transfer in coated sorber beds: An analytical solution. Int. J. Refrig.

Wu, W.D., Zhang, H., Sun, D.W., 2009. Mathematical simulation and experimental study of a modified zeolite 13X-water adsorption refrigeration module. Appl. Therm. Eng. 29 (4), 645–651.

Wakao, N., Kagei, S., 1982. Heat and mass transfer in packed beds, 1. Taylor & Francis.

K. Fayazmanesh and M. Bahrami, "Consolidated composite adsorbent containing graphite flake for sorption cooling systems," 2017.

Bahrehmand, H., Khajehpour, M., Bahrami, M., 2018. Finding optimal conductive additive content to enhance the performance of coated sorption beds : An experimental study. Appl. Therm. Eng. 143 (May), 308–315.

Bahrehmand, H., Khajehpour, M., Bahrami, M., 2018. Finding optimal conductive additive content to enhance the performance of coated sorption beds: An experimental study. Appl. Therm. Eng. 143 (July), 308–315.

A. Asghar, A. Aziz, A. Raman, W. Mohd, and A. Wan, "A Comparison of Central Composite Design and Taguchi Method for Optimizing Fenton Process," vol. 2014, 2014.

Box, G.E.P., Behnken, D.W., 1960. Some New Three Level Designs for the Study of Quantitative Variables. Technometrics 2 (4), 455–475.

Sapienza, A., Santamaria, S., Frazzica, A., Freni, A., 2011. Influence of the management strategy and operating conditions on the performance of an adsorption chiller. Energy 36 (9), 5532–5538.

Freni, A., Bonaccorsi, L., Calabrese, L., Caprì, A., Frazzica, A., Sapienza, A., 2015. SAPO-34 coated adsorbent heat exchanger for adsorption chillers. Appl. Therm. Eng. 82, 1–7.

A. Sharafian and others, "Effects of adsorbent mass and number of adsorber beds on the performance of a waste heat-driven adsorption cooling system for vehicle air conditioning applications," pp. 481–493, 2016.

U. Wittstadt et al., "A novel adsorption module with fi ber heat exchangers : Performance analysis based on driving temperature differences," vol. 110, pp. 154–161, 2017.

A. Freni, "An advanced solid sorption chiller using SWS-1L," vol. 27, pp. 2200–2204, 2007.

Dawoud, B., Höfle, P., Chmielewski, S., 2010. Experimental Investigation of the Effect of Zeolite Coating Thickness on the Performance of a novelZeolite-Water Adsorption Heat Pump Module. In: Proc. Tenth Int. Conf. Enhanc. Build. Oper, pp. 1–8.

Aristov, Y.I., Sapienza, A., Ovoshchnikov, D.S., Freni, A., Restuccia, G., 2010. Reallocation of adsorption and desorption times for optimisation of cooling cycles Optimisation des cycles de refroidissement par modification ´es d ' adsorption et de de ´sorption des dure. Int. J. Refrig. 35 (3), 525–531.

Soloukhin, R.I., Martynenko, O.G., 1985. Unified analysis and solutions of heat and mass diffusion. International Journal of Heat and Mass Transfer 28 (9), 1791.

Mikhailov, M.D., Özişik, M.N., 1986. Transient conduction in a three-dimensional composite slab. Int. J. Heat Mass Transf. 29 (2), 340–342.

Mikhailov, M.D., Vulchanov, N.L., 1983. Computational Procedure for Sturm-Liouville Problems. J. Comput. Phys. 50, 323–336.